Compressive Coherence Sensing

Daniel L. Marks
The Duke Imaging and Spectroscopy Program, Department of Electrical and Computer Engineering, Duke University, 130 Hudson Hall, Durham NC 27708

Ashwin Wagadarikar
The Duke Imaging and Spectroscopy Program, Department of Electrical and Computer Engineering, Duke University, 130 Hudson Hall, Durham NC 27708

David J. Brady
The Duke Imaging and Spectroscopy Program, Department of Electrical and Computer Engineering, Duke University, 130 Hudson Hall, Durham NC 27708

Abstract

The coherence function [1] of a stationary, ergodic electromagnetic field is the complete description of its second-order statistics [2, 3]. In a two-dimensional aperture, this function comprises the correlations between all pairs of points, so that the coherence is a four-dimensional function. While coherence is a rich source of sensing data, it is almost always impractical to measure the entire four-dimensional function. Compressive sensing [4, 5, 6] is a means by which one may accurately reconstruct an image sampling only a small fraction of the coherence samples. This is accomplished by imposing a sparsity constraint on the possible reconstructed images. If the data is such that the reconstructed image satisfies the sparsity constraint, the object can be reconstructed with an exceedingly small probability of error given a sufficient amount of data is sampled. This approach may enable new coherence instruments that infer object properties without exhaustive coherence data sampling. In this paper the framework of compressed coherence sensing is presented, and an experimental demonstration of compressed coherence sensing of a simple object through turbulence is presented.

1. COHERENCE SENSING

Partial coherence is a seldom exploited property of the electromagnetic field for remote sensing and image formation. Most instruments are imaging instruments and treat the formed image as incoherent and do not attempt to infer coherence properties of the source from the image. However, coherence is a potentially rich source of information that could be used for imaging, for example imaging through turbulence. The coherence function is the complete description of the second-order statistics of the electromagnetic field. In a two-dimensional aperture, the coherence is a four-dimensional function comprising the correlations between every pair of points in the aperture. Unfortunately, the size of the coherence function is often an impediment to its use in image formation, as in general a large portion of this function must be measured to produce an

accurate image. If the amount of coherence data necessary for quality image formation could be reduced, coherence-sensing instruments might be more practical. We propose compressive sensing as a means of inferring accurate images from limited coherence data. Compressive sensing succeeds because the image is restricted by sparsity constraints to possible images that are accurately reconstructed by a minimum of coherence samples. To demonstrate the utility of our approach with an experiment, we reconstruct using compressive sensing techniques an incoherent object through synthetic turbulence by sampling the coherence using an interferometer. Our demonstration shows that, within limits, it is possible to reconstruct an object from a limited set of coherence samples.

The coherence of the electromagnetic field in the scalar approximation is described by the cross-spectral density

$$W(x_1, y_1, x_2, y_2, \omega) = \langle E(x_1, y_1, \omega)^* E(x_2, y_2, \omega) \rangle \tag{1}$$

where $E(x, y)$ is a quasimonochromatic stochastic electromagnetic field centered around frequency ω . From the van Cittert-Zernike theorem [7, 8] we can derive the following propagation law of the field radiated from an incoherent source of spectral density $S(\mathbf{r}, \omega)$:

$$\begin{aligned} W(x_1', y_1', x_2', y_2', \omega) = \int dx\, dy \tfrac{S(x,y,\omega)}{iz^2} \\ \exp\left[\tfrac{-2i\omega}{c}\left((x_2' - x_1')\tfrac{x}{z} + (y_2' - y_1')\tfrac{y}{z}\right)\right] \end{aligned} \tag{2}$$

Simply stated, the two-dimensional Fourier transmission of the power spectral density is the cross-spectral density in the far field as a function of the difference between the two coordinates that are correlated. To recover the spectral density of the source, the remote cross-spectral density may be measured as a function of spatial coordinate differences $x_2' - x_1'$ and $y_2' - y_1'$ about a central point using an interferometer and then inverse Fourier transformed to find the power spectral density.

If isoplanatic turbulence with an optical path delay $d(x', y')$ is present between the source and receiver, the cross-spectral density becomes

$$\begin{aligned} W(x_1', y_1', x_2', y_2', \omega) = \exp\left[\tfrac{i\omega}{c}\left(d(x_1', y_1') - d(-x_2', -y_2')\right)\right] \\ \int dx\, dy \tfrac{S(x,y,\omega)}{iz^2} \exp\left[\tfrac{-2i\omega}{c}\left((x_2' - x_1')\tfrac{x}{z} + (y_2' - y_1')\tfrac{y}{z}\right)\right] \end{aligned} \tag{3}$$

The phase introduced into the cross-spectral density distorts the resulting image if the van Cittert-Zernike theorem is used to inverse the cross-spectral density. Unlike a conventional image of an object in turbulence using a lens, the cross-spectral density measurement contains phase data that includes the turbulence phase.

We use an instrument called the rotational shearing interferometer (RSI) [9, 10, 11, 12, 13, 14] to measure the cross-spectral density, as presented in Fig. 1. This interferometer consists of a beams plitter and two folding mirrors. The beam splitter divides the wavefront to be sampled into two. Each of the split fields is reflected and rotated by the roof prism, so that the recombined fields have a relative rotation. The superimposed fields are measured on a sensor array. The delay of one arm of the interferometer is varied to allow phase-shifting to find the phase-resolved cross-spectral density.

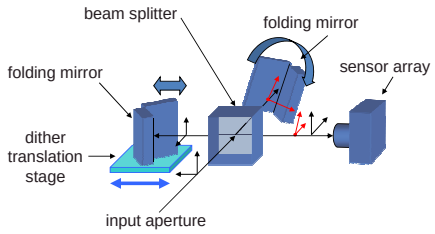

Figure 1: The rotational shearing interferometer.

If we consider a stochastic field $E(x', y')$ incident on the rotational shearing interferometer, the cross-spectral density $W'(\eta, \xi, \omega)$ sampled at a position η, ξ on the sensor is given by

$$\begin{aligned} W'(\eta, \xi, \omega) = \langle & E(\eta \cos\theta + \xi \sin\theta, -\eta \sin\theta + \xi \cos\theta)^* \\ & E(\eta \cos\theta - \xi \sin\theta, \eta \sin\theta + \xi \cos\theta)^* \rangle = \\ & W(\eta \cos\theta + \xi \sin\theta, -\eta \sin\theta + \xi \cos\theta, \eta \cos\theta - \xi \sin\theta, \eta \sin\theta + \xi \cos\theta) \end{aligned} \tag{4}$$

given that one arm of the interferometer rotates the field $+\theta$ radians and the other arm rotates the field $-\theta$ radians. Expressing Eq. 3 as a function of η and ξ this becomes

$$\begin{aligned} & W'(\eta, \xi, \omega) = \\ & \quad \exp\left[\tfrac{i\omega}{c}\left(d(\eta \cos\theta + \xi \sin\theta, -\eta \sin\theta + \xi \cos\theta) - \right.\right. \\ & \quad \left.\left. d(\eta \cos\theta - \xi \sin\theta, \eta \sin\theta + \xi \cos\theta)\right)\right] \\ & \quad \int dx\, dy \tfrac{S(x,y,\omega)}{iz^2} \exp\left[\tfrac{4i\omega}{c}\left(\xi \sin\theta \tfrac{x}{z} - \eta \sin\theta \tfrac{y}{z}\right)\right] \end{aligned} \tag{5}$$

Disregarding the turbulence $d(x', y')$, the cross-spectral density measured by the RSI is the Fourier transform of the source intensity, rotated by 90 degrees and scaled by $1/2 \sin\theta$. Because of this, the RSI is an ideal interferometer to use to reconstruct incoherent sources. The turbulence adds an extra phase term to the measurement that distorts the estimate of the source intensity. However, the cross-spectral density in the absence of turbulence has Hermitian symmetry, that is $W'(\eta, \xi, \omega) = W'(-\eta, -\xi, \omega)^*$ being the Fourier transform of a real function, the spectral density of the source. If the angle $\theta \neq \pi/2$, the turbulence does not necessarily have Hermitian symmetry. Because of this disparity, the turbulence phase can be distinguished from the phase due to the source itself. Compressive sensing techniques are used to find the turbulence phase and the source spectral density, partially based on this distinction.

2. COMPRESSIVE SENSING

As previously mentioned, the coherence function is four-dimensional being the correlations of every pair of 2-D points in an aperture, while the RSI samples only a two-dimensional subset of this coherence function. The previous section presented a model for the coherence function of an incoherent source in the presence of turbulence. To infer the source spectral density [15, 16, 17, 18] and the turbulence from this subset of the coherence [19, 20], we employ algorithms used in compressive sensing, modifying them for improved performance in the presence in turbulence.

The conventional compressive sensing problem is framed as: find the solution that minimzes $\| \mathbf{y} - \mathbf{A}\mathbf{x} \|^2 + \tau ||\mathbf{x}| |_0$. In this context, $\mathbf{y}$ is a measurement vector, $\mathbf{x}$ is the data vector to be inferred, and $\mathbf{A}$ is a linear transformation between the data and measurement vectors. The constraint $\| \mathbf{y} - \mathbf{A}\mathbf{x} \|^2$ is a conventional least-squares constaint that ensured that the data conforms to the measurements. The other constraint that minimizes $||\mathbf{x}| |_0$ simply counts the number of nonzero elements in the vector $\mathbf{x}$. This is a sparsity constraint based on the 0-norm (ℓ_0) that strongly restricts the possible solutions. This constraint might be useful, for example, if $\mathbf{x}$ represents image samples and it is desired to have the minimum number of pixels be nonzero. Unfortunately as posed this problem is NP so that the computational effort is too great for any resonably sized image.

Rather than solve the ℓ_0 problem we can pose it as a different problem based on the ℓ_1-norm: minimizing $\| \mathbf{y} - \mathbf{A}\mathbf{x} \|^2 + \tau ||\mathbf{x}| |_1$. The ℓ_1-norm is a convex norm, and the sum of these norms is likewise a convex functional. Therefore many convex optimization methods are available that can find the minimum solution which is unique. One of the basic results of compressive sensing is that minimizing ℓ_1 always provides the same answer that minimizing ℓ_0 would select given that the number of measurements is sufficient and the forward operator satisfied certain conditions [21, 22]. This result makes certain compressive sensing computations practical and allows analysis of the reconstruction of sparse data vectors.

For coherence sensing, $\mathbf{y}$ is a vector of measured coherence samples, $\mathbf{x}$ is a desired image to estimate, and $\mathbf{A}$ is a linear transformation that describes the propagation of partially coherent light, in this case the van Cittert-Zernike theorem including turbulence. Conventional reconstruction of an image might minimize the 2-norm of the vector $\mathbf{x}$ which is Tikhonov regularization. Unfortunately this constraint tends to produce poor images when little data is available because ℓ_2-norm restricts only the total energy in the image and not the concentration of this energy throughout the image. On the other hand, typical images do not consist of power distributed randomly over the image, but rather of discrete objects and surfaces that tend to have features that cluster in certain pixels. The ℓ_1-norm tends to produce these images as it concentrates the energy of the image into discrete points. Therefore the ℓ_1-norm can produce interesting and useful imagery under more realistic constraints as well as be practical to compute.

There are many procedures for finding the minimum of the ℓ_1-norm compressive sensing problem. The algorithm used here is two-step iterative shrinking

and thresholding [23] (TwIST). Each iteration this algorithm alternates between a shrinking step that reduces the least-squares penalty and a thresholding that reduces the ℓ_1-norm. When the minimum is reached to a particular accuracy, the directions of the correction gradient for the least-squares and the ℓ_1 norm oppose as is needed in any Lagrange multiplier constrained problem, and the iteration may be terminated.

Geometrically, this process has an appealing interpretation. The surface of a constant squared-error is a hypersphere. On the other hand, the surface of constant ℓ_1 is the surface of a polytope bounded by hyperplanes called the ℓ_1 ball. The solution is typically the intersection between the hypersphere and a corner of the ℓ_1 ball. Because the corners of the ℓ_1 ball are sharp, small errors in the data tend to not change which elements of the vector $\mathbf{x}$ are nonzero, as this would involve switching the solution to another corner where the ℓ_1 ball touches the sphere. Therefore the sparsity constraint is robust against error.

A block diagram of the modified TwIST algorithm is presented in Fig. 2. The least-squares constraint is enforced using gradient-descent. The ℓ_1 constraint is enforced by soft-thresholding the elements of $\mathbf{x}$ that places the solution on a corner of the ℓ_1 ball. However, without modification the algorithm does not account for the turbulence phase. The turbulence phase effectively modifies the propagation operator $\mathbf{A}$. Therefore each iteration both the image and turbulence phase are estimated. The first step is a shrinking step that applies the least-squared constraint to the Fourier transform of the data. The current estimate of the phase is applied to the Fourier data estimate, and the data is converted to the spatial domain using the inverse Fourier transform to form an image estimate. The estimated intensity of the spatial-domain image is soft-thresholded to apply the sparsity constraint. The Fourier transform returns the spatial-domain image to the Fourier domain data. The phases of the sparsely constrained image and the current turblence-aberrated image are subtracted to form a new turbulence phase estimate. The data is then underrelaxed to stabilize the iterations. Iteration continues until the iterations produce a minimal change.

3. AN EXPERIMENTAL DEMONSTRATION

To demonstrate the use of compressive sensing to correct turbulence, we observe light emitting diodes through an aberrating phase screen using the rotational shearing interferometer, as detailed in Fig. 3. The LEDs emitted wavelengths in the yellow region of the spectrum, and has their plastic lenses sanded off to nearly the LED chip die to produce isotropic and incoherent radiation. These LEDs were collimated by a lens to place their image at infinity as would occur for stellar imaging. An iris eliminates vignetting effects from the collimation lens. A phase distortion plate is placed behind the iris to produce an instance of the phase distortion caused by turbulence. This plate was constructed by dripping polydimethylsiloxane (Sylgard 184) silicone onto a microscope slide and then heating with with a heat gun to cure it quickly before the surface became more uniformly flat. A second lens relays the partially coherent aberrated field to the entrance of the RSI. The RSI collected the intensity interferograms as the delay between the two arms of the interferometer was varied. The interferograms at

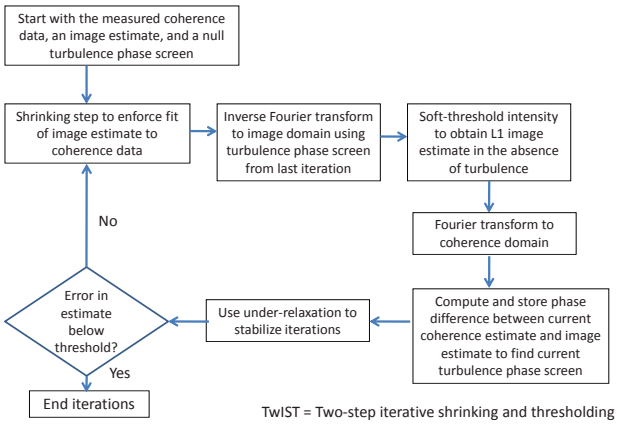

Figure 2: A block diagram of the compressive sensing algorithm used to find the unaberrated image and a turbulence estimate.

four delays I_0,$I_{\pi/2}$,I_π,$I_{3\pi/2}$ with phases separated by $\pi/2$ were summed to find the coherence estimate using the formula $W = I_0 + iI_{\pi/2} - I_\pi - iI_{3\pi/2}$. The modified TwIST algorithm was applied to the coherence estimate. The constant τ was chosen to be the average intensity of all the points in the image with an intensity more than 10% of the maximum intensity in the image. This ensured that the image would be sharpened with the soft-thresholding, but not overly so as to remove significant features from the data. The forward operator of the TwIST algorithm was weighted to favor low frequencies in the image as these are less affected by turbulence.

The results of the experiment are in Fig. 4. The image of the LEDs assuming no distortion is present is in part (c). The aberration substantially distorts the image. The estimate of the coherence function without the turbulence is part (a). The real part of the complex phase of the estimated phase screen of the distortion is part (b). This shows that the phase screen and the object can be jointly estimated. Part (d) is the estimated object. The algorithm clearly improves the quality of the image, whereas it would be hard to discern the three LEDs from the original aberrated image.

As a control experiment, we performed the same imaging but without a phase distortion plate as shown in Fig. 5. Part (a) is the reconstructed coherence function without turbulence, which resembles that of Fig. 4. The phase of the distortion is estimated to be almost zero in part (b). Part (c) is the image of the LEDs directly computed from the unchanged sampled coherence data. Part (d) is the image produced by the algorithm. Because of the L1 constraint, the algorithm improves the image of the LEDs slightly, sharpening the points. The control experiment suggests that the algorithm does not merely deconvolve the

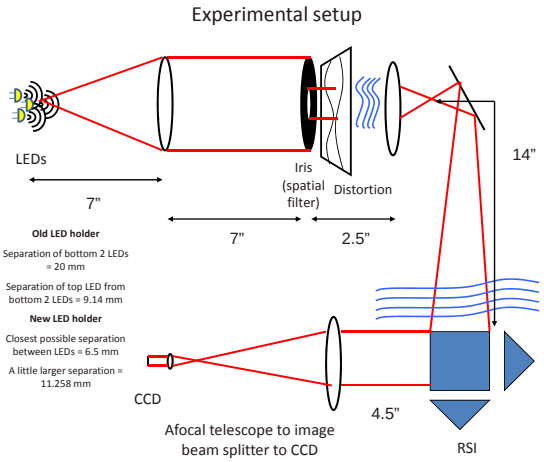

Figure 3: Diagram of the setup to measure the cross-spectral density from LEDs with a phase distortion.

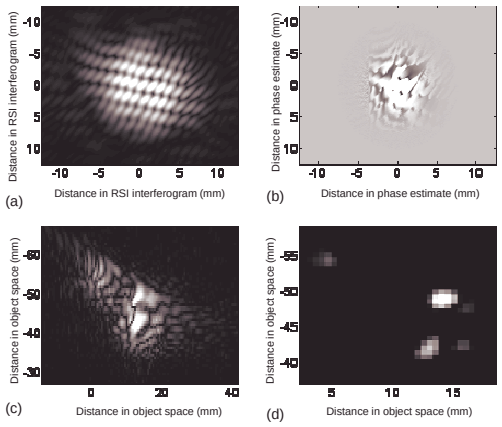

Figure 4: Results of compressive sensing reconstruction of three LEDs aberrated by turbulence. (a) The reconstructed coherence function of the LEDs without turbulence. (b) The estimated phase of the aberration. (c) The image neglecting turbulence, showing the distortion produced by turbulence. (d) The estimate of the source intensity without turbulence.

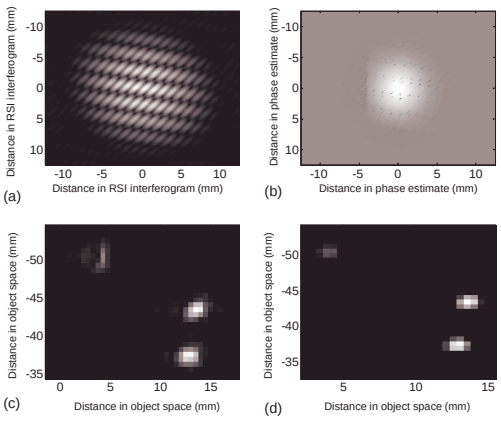

Figure 5: Results of a control experiment of compressive sensing reconstruction of three LEDs not aberrated by turbulence. (a) The reconstructed coherence function of the LEDs. (b) The estimated phase of the aberration, which is close to null because no turbulence is present. (c) The image of the original source. (d) The estimate of the source intensity, which improves the image quality because the L1 constraint sharpens the points slightly.

image directly, but actually estimates the phase and applies this phase to the sampled coherence to produce an improved image.

References

[1] D. J. Brady, *Optical Imaging and Spectroscopy.* New York: Wiley, 2009.

[2] L. Mandel and E. Wolf, *Optical Coherence and Quantum Optics.* Cambridge: Cambridge University Press, 1995.

[3] J. Goodman, *Statistical Optics.* New York: John Wiley & Sons, 1985.

[4] D. L. Donoho, "Compressed sensing," *IEEE Trans. Inf. Theory*, vol. 52, no. 4, pp. 1289–1306, 2006.

[5] E. J. Candes and T. Tao, "Near-optimal signal recovery from random projections: Universal encoding strategies?" *IEEE Trans. Inf. Theory*, vol. 52, no. 12, pp. 5406–5426, 2006.

[6] E. J. Candes, J. K. Romberg, and T. Tao, "Stable signal recovery from incomplete and inaccurate measurements," *Comm. Pure Appl. Math.*, vol. 59, pp. 1207–1223, 2006.

[7] P. H. Van Cittert, "Die wahrscheinliche schwingungsventeilung in einer von einer lichtquelle direkt oder mittels einer linse beleuchten ebene," *Physica*, vol. 1, pp. 201–208, 1934.

[8] F. Zernike, "The concept of degree of coherence and its application to optical problems," *Physica*, vol. 5, pp. 785–796, 1938.

[9] M. Murty and E. Hagerott, "Rotational-shearing interferometry," *Appl. Opt.*, vol. 5, no. 4, pp. 615–619, 1966.

[10] F. Roddier, C. Roddier, and J. Demarcq, "A rotation shearing interferometer with phase-compensated roof prisms," *J. Opt. (Paris)*, vol. 11, pp. 149–152, 1978.

[11] C. Roddier, F. Roddier, and J. Demarcq, "Compact rotational shearing interferometer for astronomical applications," *Opt. Eng.*, vol. 28, no. 1, pp. 66–70, 1989.

[12] C. Roddier and F. Roddier, "High angular resolution observations of Alpha Orionis with a rotation shearing interferometer," *Astrophys. J.*, vol. 270, pp. L23–L26, 1983.

[13] F. Roddier, "Interferometric imaging in optical astronomy," *Physics Reports*, vol. 17, pp. 97–166, 1988.

[14] E. Ribak, C. Roddier, F. Roddier, and J. B. Breckinridge, "Signal to noise considerations in white-light holography," *Appl. Opt.*, vol. 27, pp. 1183–1186, 1988.

[15] K. Itoh and Y. Ohtsuka, "Interferometric imaging of a thermally luminous two-dimensional object," *Opt. Comm.*, vol. 48, no. 2, pp. 75–79, 1983.

[16] K. Itoh, T. Inoue, and Y. Ichioka, "Interferometric spectral imaging and optical three-dimensional Fourier transformation," *Jap. J. Appl. Phys.*, vol. 29, pp. 1561–1564, 1990.

[17] K. Itoh, T. Inoue, T. Yoshida, and Y. Ichioka, "Interferometric multispectral imaging," *Appl. Opt.*, vol. 29, pp. 1625–1630, 1990.

[18] K. Itoh and Y. Ohtsuka, "Fourier-transform spectral imaging: retrieval of source information from three-dimensional spatial coherence," *J. Opt. Soc. Am. A*, vol. 3, pp. 94–100, 1986.

[19] R. G. Paxman, T. J. Schulz, and J. R. Fienup, "Joint estimation of object and aberrations using phase diversity," *J. Opt. Soc. Am. A*, vol. 9, pp. 1072–1085, 1992.

[20] J. Primot, G. Rousset, T. Marais, and J. C. Fontanella, "Deconvolution of turbulence-degraded images from wavefront sensing," *Proc. SPIE*, vol. 1130, pp. 29–32, 1989.

[21] A. Juditsky and A. S. Nemirovski, "On verifiable sufficient conditions for sparse signal recovery via l1 optimization," 2008, available http://www.citebase.org/abstract?id=oai:arXiv.org:0809.2650.

[22] K. Lee and Y. Bresler, "Computing performance guarantees for compressed sensing," in *International Confererence on Acoustics, Speech and Signal Processing, 2008.*, Apr 2008, pp. 5129–5132.

[23] J. M. Bioucas-Dias and M. A. T. Figueiredo, "A new twist: two-step iterative shrinkage/thresholding algorithms for image restoration," *IEEE. Trans. Image Proc.*, vol. 16, no. 12, pp. 2992–3004, Dec. 2007.